Generation of intermittent ion acoustic waves in whistler-mode turbulence

S. Saito, Y. Nariyuki, and T. Umeda

Generation of intermittent ion acoustic waves in whistler-mode turbulence

S. Saito,[1,a)] Y. Nariyuki,[2,b)] and T. Umeda[3,c)]

[1]*Graduate School of Science, Nagoya University, Furo-cho, Chikusa-ku, Nagoya, Aichi 464-8601, Japan*
[2]*Faculty of Human Development, University of Toyama, 3190, Gofuku, Toyama 930-8555, Japan*
[3]*Institute for Space-Earth Environmental Research, Nagoya University, Furo-cho, Chikusa-ku, Nagoya, Aichi 464-8601, Japan*

A two-dimensional, fully kinetic, electromagnetic, particle-in-cell simulation in a magnetized collisionless plasma has been performed, demonstrating the generation of intermittent ion acoustic waves in finite-amplitude whistler-mode turbulence. The self-consistent simulation shows that ion/ion acoustic instability can be driven as a consequence of the nonlinear evolution of whistler-mode turbulence. The instability triggering the generation of ion acoustic waves occurs intermittently in several local regions. We propose that the nonlinear development of the phase-space density that drives kinetic instabilities must be analyzed with greater care if the dissipation of plasma turbulence is to be understood. © 2017 Author(s). All article content, except where otherwise noted, is licensed under a Creative Commons Attribution (CC BY) license (http://creativecommons.org/licenses/by/4.0/). [http://dx.doi.org/10.1063/1.4990443]

I. INTRODUCTION

Forward cascade in magnetohydrodynamics (MHD) turbulence plays an important role in the generation of plasma turbulence at scales smaller than the ion inertial length and ion Larmor radius. This small-scale turbulence, or alternatively kinetic turbulence because the MHD approximation is expected to be broken there, has been considered as an energy sink of solar-wind turbulence. At scales for kinetic turbulence, analyses of solar-wind observations have yielded a power-law spectrum for the energy of magnetic fluctuations that is steeper than that for MHD turbulence. The steeper magnetic energy spectrum suggests that the kinetic nature of the fluctuations involves different cascade processes from that of MHD turbulence. In particular, both kinetic Alfvén and whistler modes are believed to be crucial in transferring the energy of fluctuations from ion kinetic scales to electron kinetic scales. These fluctuations are finally dissipated by wave-particle interactions at the kinetic scales.

Several observations have shown evidence for kinetic Alfvén-mode turbulence at ion gyroscales.[1–3] Specifically, Sahraoui *et al.*[3] reported kinetic Alfvén modes present at electron gyroscales from solar-wind observations made during the Cluster space mission, whereas the kinetic Alfvén-mode turbulence is not present at these scales owing to resonant dissipation at ion kinetic scales.[4] Moreover Sahraoui *et al.*[3] evidenced at electron gyroscales a steeper gradient in the spectra related to the dissipation of kinetic Alfvén-mode turbulence.

In contrast, the whistler mode is nearly undamped even at ion kinetic scales because the dissipation rate of the cyclotron and Landau resonance is weak.[5] Several observations indicate that kinetic-scale fluctuations are of whistler-mode type.[6–8] The recent analysis from four-point magnetometry on the Magnetospheric Multiscale mission directly determined the dispersion relation for magnetic fluctuations at electron inertial length and concluded that solar-wind turbulence at electron kinetic scales is primarily composed of the whistler mode propagating obliquely with respect to the background magnetic field.[8] Their observations support a scenario that the energy of fluctuations cascading from the MHD turbulence transitions into whistler-mode turbulence at kinetic scales.

At electron kinetic scales, whistler-mode turbulence dissipates through the cyclotron and Landau resonances of the electrons. These resonant interactions depend on the propagation angle of the whistler fluctuation, so a preferred resonance in whistler-mode turbulence depends on the direction of cascading of fluctuation energy. Several theoretical and simulation studies[9–17] have identified that anisotropic cascades in whistler-mode turbulence at electron kinetic scales efficiently transfer the energy of fluctuations into a quasi-perpendicular propagating whistler mode. Therefore, the preferred resonance in whistler-mode turbulence is the Landau process that scatters electrons in the magnetic field direction at electron kinetic scales.[12,13] At electron kinetic scales, ions can also be scattered in whistler-mode turbulence[18,19] because quasi-perpendicular propagating whistlers at frequencies close to the lower hybrid frequency scatter ions efficiently transverse to the field direction by their electrostatic component.[20,21] These resonance scatterings of electrons and ions dissipate whistler-mode turbulence at electron kinetic scales.

However, we expect that the kinetic processes bring about not only dissipation of linear modes through the cyclotron and Landau resonances at electron kinetic scales but also development and deformation of the phase-space density at ion kinetic scales. The deformation of phase-space density in the nonlinear development of kinetic turbulence causes several kinetic instabilities that lead to particle

a)Electronic mail: s.saito@nagoya-u.jp
b)Electronic mail: nariyuki@edu.u-toyama.ac.jp
c)Electronic mail: umeda@isee.nagoya-u.ac.jp

scattering. From an analysis of a fully kinetic particle-in-cell simulation, we propose that the nonlinear development of whistler-mode turbulence drives ion/ion acoustic instability which leads to density fluctuations at electron kinetic scales. The purpose of this study is to investigate the role of nonlinear-evolving whistler-mode turbulence played in enhancing ion/ion acoustic instability.

II. SIMULATION

A. Initial condition

To analyze the nonlinear development of whistler-mode turbulence, we implemented a two-dimensional particle-in-cell simulation code that uses the zigzag method[22] and the Boris method[23] to compute the electric current and the motion of charged particles, respectively. The spatial size of the simulation box (L_x, L_y) was $(20.48\lambda_i, 20.48\lambda_i)$, where λ_i is the ion inertial length. The number of spatial grids is 4096 $\times$ 4096. The number of ion and electron pairs in a cell is 256, and hence the total number of pairs is about 4.29×10^9. The time resolution Δt was set to $5.59 \times 10^{-5}\Omega_i^{-1}$, where Ω_i is the ion cyclotron angular frequency. The ratio of the ion plasma frequency to the ion cyclotron frequency was set to $\omega_i/\Omega_i = 44.7$. These frequencies are defined by the initial density n_o and the initial background magnetic field $\mathbf{B}_o$. The Alfvén velocity $v_A = (\Omega_i/\omega_i)c$, with c being the speed of light, normalized by the initial ion thermal speed v_{ti} was set to $v_A/v_{ti} = 4.47$. Note that we assume the mass ratio between the ion and electron to be $m_i/m_e = 100$ and the ion thermal speed normalized by the speed of light to be $v_{ti}/c = 0.005$ at $t = 0$ to reduce the calculation cost. The ratio of the initial temperatures of ions and electrons was set to $T_i/T_e = 1$, and the beta values for both ions and electrons were $\beta_i = \beta_e = 0.1$. The background magnetic field $\mathbf{B}_o$ was along the x direction.

Similar to our previous studies [e.g., Ref. 13] whistler waves (totaling 42 modes in the simulation box) were allocated random wave phases at t = 0. The initial parallel (or perpendicular) wavenumbers of the generated waves were set to $k_{x(y)}\lambda_i = \pm0.306, \pm0.613$, and ±0.9203. Pure parallel propagating modes ($k_y = 0$) were also generated. The frequency of each mode was derived from the linear dispersion relation for whistler waves in the cold plasma approximation.[24] All modes

have an almost-equal energy of magnetic fluctuations. The total energy of magnetic fluctuations at $t = 0$ is about 10% of the background magnetic field energy. We excited fluctuations in the electric current density $\delta\mathbf{J} = q_i n_i \mathbf{v}_{d,i} + q_e n_e \mathbf{v}_{d,e}$ corresponding to the fluctuations of the applied magnetic field, which satisfy Faraday's and Ampère's equations. Here, q_i (q_e) is the electric charge of the ion (electron), n_i (n_e) is the density of ions (electrons), and $\mathbf{v}_{d,i}$ ($\mathbf{v}_{d,e}$) is the ion (electron) drift velocity carrying the electric current. Whereas the electric and density fluctuations were required to produce self-consistent whistler waves, we neglected these contributions in generating the initial waves. We believe that these small contributions are negligible because the calculation provides self-consistent adjustments to the waves within a relatively short period, which may be shorter than a few ion plasma periods. Having neglecting the small initial contributions, the turbulence was confirmed to have the properties of whistler modes soon after this self-consistent development.[13]

B. Results

Figure 1 illustrates the wavenumber spectra of the fluctuations in magnetic energy $|\delta\mathbf{B}|^2/B_o^2$ as a function of k_x and k_y at $\Omega_i t = 5.59, 11.18$, and 16.77. As described in Sec. II A, the initial magnetic-field fluctuations were set at wavenumbers $k_x\lambda_i < 1$ and $k_y\lambda_i < 1$. The imposed fluctuations cascade preferentially to those of larger wavenumbers perpendicular to the direction of background magnetic field. Whereas previous simulation studies[12,13] reported an anisotropic wavenumber spectrum for whistler-mode turbulence at electron kinetic scales, the simulation result shown here evidences an anisotropy even at ion kinetic scales. Obliquely propagating whistler waves are dominant over ion-to-electron kinetic scales, indicating that whistler-mode turbulence is fundamentally compressible even at ion kinetic scales because oblique whistler waves are compressible in nature.

Figure 2 illustrates the wavenumber spectra of ion density fluctuations $|\delta n_i|^2/n_o^2$ as functions of k_x and k_y (upper panels) and as a function of k_x at $k_y\lambda_i = 0.92$ (lower panels) at $\Omega_i t = 5.59, 11.18$, and 16.77. The spectra of the ion-density fluctuations are similar to those of the magnetic-field fluctuations (Fig. 1) within $k_x\lambda_i < 5$. However, it is evident that the ion-density fluctuation for $k_x\lambda_i > 10$ is generated at
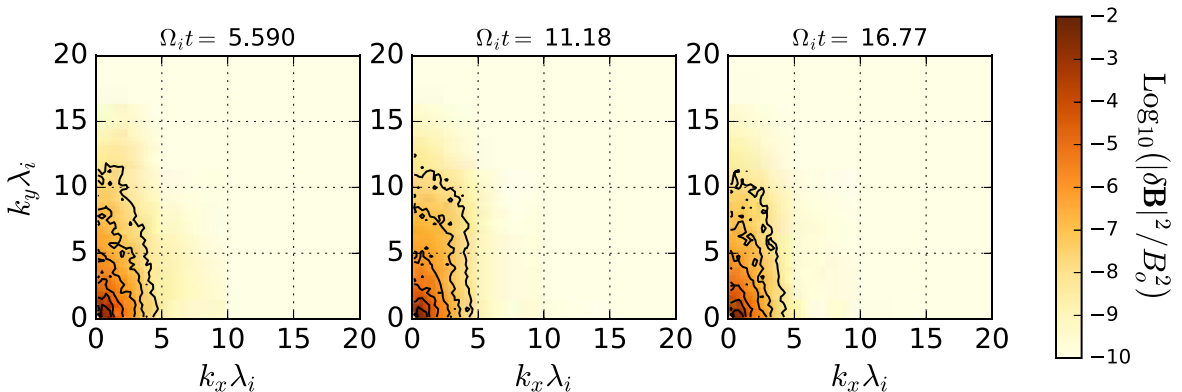

FIG. 1. Wavenumber spectra of magnetic fluctuations $|\delta\mathbf{B}(k_x, k_y)|^2$ at $\Omega_i t = 5.59, 11.18$, and 16.77. Here, $|\delta\mathbf{B}(k_x, k_y)|^2 = |\delta\mathbf{B}_x(k_x, k_y)|^2 + |\delta\mathbf{B}_y(k_x, k_y)|^2 + |\delta\mathbf{B}_z(k_x, k_y)|^2$. The fluctuations in magnetic energy are normalized by the energy of the background magnetic field B_o.
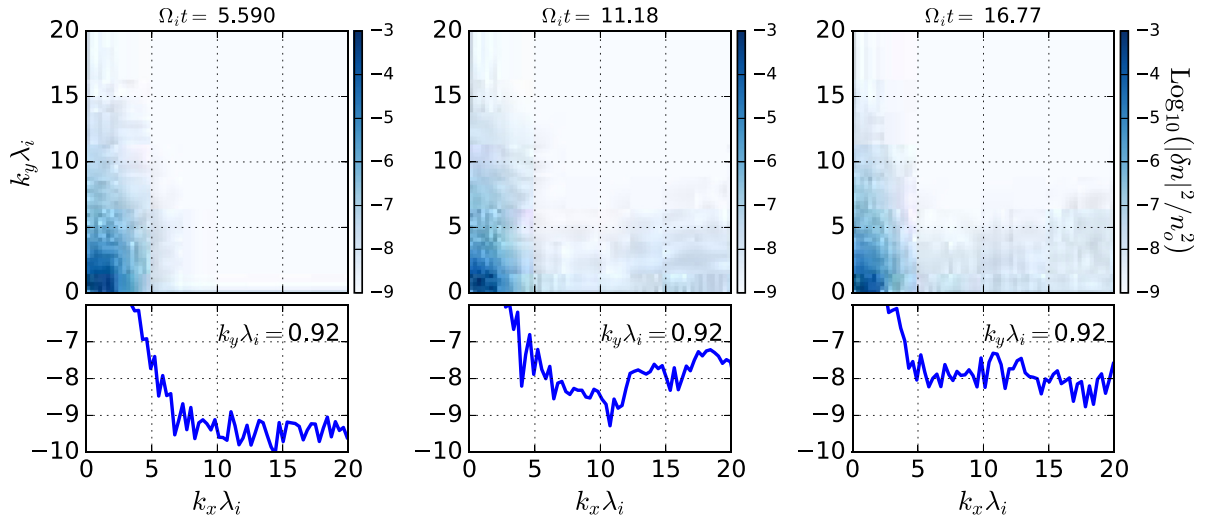
FIG. 2. (Top panels) Wavenumber spectra of ion density fluctuations normalized by the initial ion density as a function of k_x and k_y at $\Omega_i t = 5.59, 11.18$, and 16.77. (Bottom panels) Wavenumber spectra of ion density fluctuations as a function of k_x with $k_y \lambda_i = 0.92$ at $\Omega_i t = 5.59, 11.18$, and 16.77.

later times ($\Omega_i t > 11.18$). The short-scale fluctuations have wavenumbers quasi-parallel to the mean magnetic field ($k_x \gg k_y$). The corresponding magnetic-field fluctuations are absent as shown in Fig. 1. Therefore, these fluctuations are electrostatic at scales shorter than the ion inertial length λ_i.

Figure 3 illustrates the ion-density distributions n_i/n_o over the two-dimensional spatial plane at $\Omega_i t = 11.18$. The left panel plots the density distribution over the entire two-dimensional simulation box; the framed regions labeled (A), (B), and (C) are enlarged in the other three panels. Whistler-mode turbulence leads to ion-density fluctuations at ion kinetic scales because of the compressive nature of the quasi-perpendicular propagating whistler waves (left panel). The ponderomotive force of the finite-amplitude magnetic-field fluctuations also leads to the density fluctuations at the ion kinetic scales. However, as seen in panels (A)–(C), density fluctuations associated with short wavelengths of less than λ_i grow in the ion-scale density fluctuations. Also, the small-scale fluctuations have wavenumbers quasi-parallel to the mean magnetic field. These fluctuations form wave packets at a spatial scale of a few ion inertial lengths.

Figure 4 shows the ion-density distributions parallel to the background magnetic field at transverse displacements y/λ_i of 2.5, 5.0, 7.5, 10.0, 12.5, 15.0, and 17.5. The horizontal and vertical axes represent the spatial and time dimensions, respectively. Small-scale density fluctuations are seen

in several regions, for instance, around $[x/\lambda_i, \Omega_i t] = [9, 10]$ at $y/\lambda_i = 2.5$, $[8, 12]$ at $y/\lambda_i = 5.0$, and $[15, 10]$ at $y/\lambda_i = 10$. Wave packets propagate parallel or anti-parallel to the background magnetic field (x-axis). A typical life time for each packet is about a few $\Omega_i t$, but Fig. 4 shows that these wave packets grow intermittently in several regions at $\Omega_i t > 8$.

Figure 5 shows the ion phase-space density as functions of x and v_x, where the phase-space density is integrated over transverse displacements $y/\lambda_i = 1.92$ and 2.56 and normalized to f_o, which is the maximum value of the integrated phase-space density at $t = 0$. Here, x and v_x are normalized to the ion inertial length λ_i and the ion thermal speed v_{ti} at $t = 0$, respectively. The region associated with the spatial integration in the y direction includes the line plotted in the bottom panel of Fig. 4 ($y/\lambda_i = 2.5$). Perturbations in the ion velocity corresponding to the ion-density fluctuations at ion kinetic scales grow along the background magnetic field as seen at $\Omega_i t = 2.236$ (first panel). The group of ions moving along the field direction with a drift speed of $\sim -3v_{ti}$ interacts with another group of ions in the near-rest frame as seen around $x/\lambda_i = 9$ at $\Omega_i t = 6.708$ (third panel). Small-scale hole-like structures are produced between the two ion distributions at $\Omega_i t = 11.18$ (fifth panel), the spatial size of which is less than a half of λ_i. The small-scale structures correspond to the density fluctuations [labeled as (B) in Fig. 3] and seen around $[x/\lambda_i, \Omega_i t] = [9, 10]$ in the bottom panel of Fig. 4.
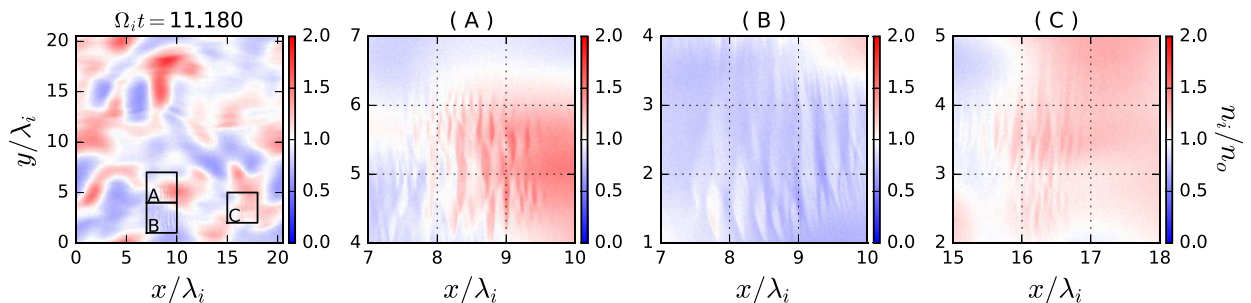

FIG. 3. (Left panel) Ion density n_i normalized by the initial ion density n_o on the whole two-dimensional plane at $\Omega_i t = 11.18$. (Panels A, B, and C) Ion density in the marked squares labeled as A, B, and C in the left panel.
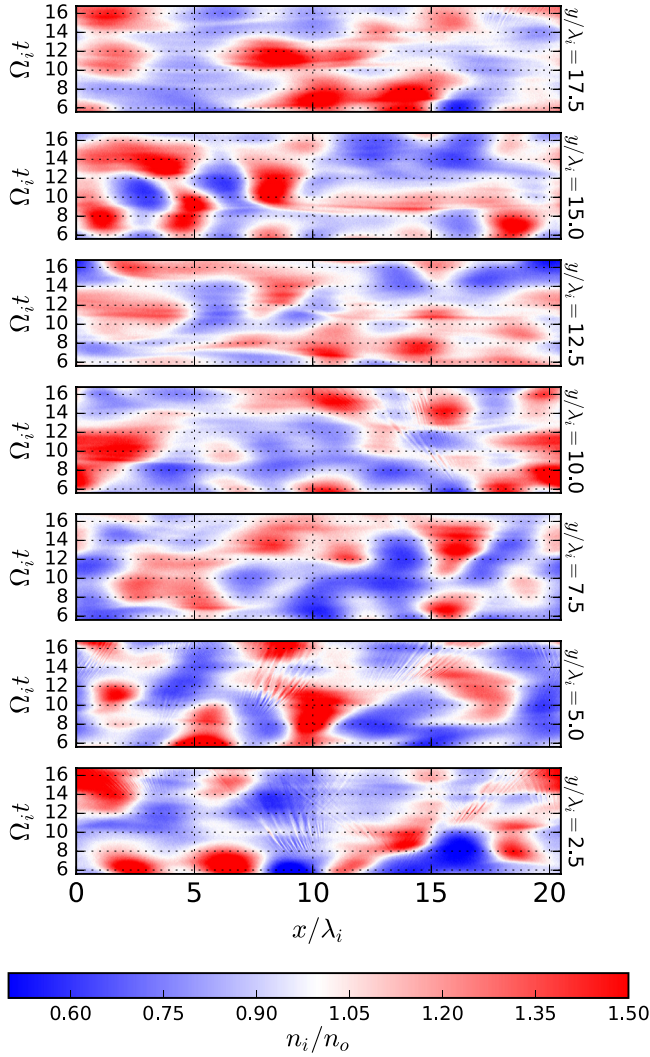
FIG. 4. Time profile of ion density distribution (n_i/n_o) along x lines at $y/\lambda_i = 2.5, 5.0, 7.5, 10.0, 12.5, 15.0,$ and 17.5. Horizontal and vertical axes correspond to the spatial (x/λ_i) and time ($\Omega_i t$) dimensions, respectively.

FIG. 5. Ion phase-space density between $y/\lambda_i = 1.92$ and 2.56 as a function of x/λ_i and v_x/v_{ti} at $\Omega_i t = 2.236, 4.472, 6.708, 8.944,$ and 11.18. The phase-space density f_i is normalized by f_o, which is the maximum value of the phase-space density at $\Omega_i t = 0$.

The top panel of Fig. 6 shows the reduced ion-velocity distributions obtained by integrating the phase-space density (Fig. 5) over the range $x/\lambda_i = 8.5$ and 9.5 at $\Omega_i t = 5.590$, $6.708, 7.826,$ and 8.944. The group of ions moving along the field direction with drift speed less than $-1.5v_{ti}$, hence constituting what we refer to as the beam component, contributes to the second peak in the ion velocity distribution. The width of the beam component is $\sim 0.5 v_{ti}$, indicating that the temperature of the beam is about $0.25 T_{i,o}$, where $T_{i,o}$ is the initial temperature of the ions. Another group of ions in the rest frame, which we refer to as the core component, has a velocity distribution deviating from a Maxwellian distribution especially for $v_x/v_{ti} > 1$ (see top panel). A rough estimate of the temperature of the core component yields $v_x \approx 0$ as $\sim 0.25 T_{i,o}$. The density ratio of the beam and core components is shown in the middle panel as a function of time between $\Omega_i t = 5.59$ and 8.944. The density of the beam and core components is calculated by integrating the reduced ion velocity distributions over a range in $v_x/v_{ti} < -1.5$ and $v_x/v_{ti} \geq -1.5$, respectively. The bottom panel shows the time history of the drift speed of the beam component which
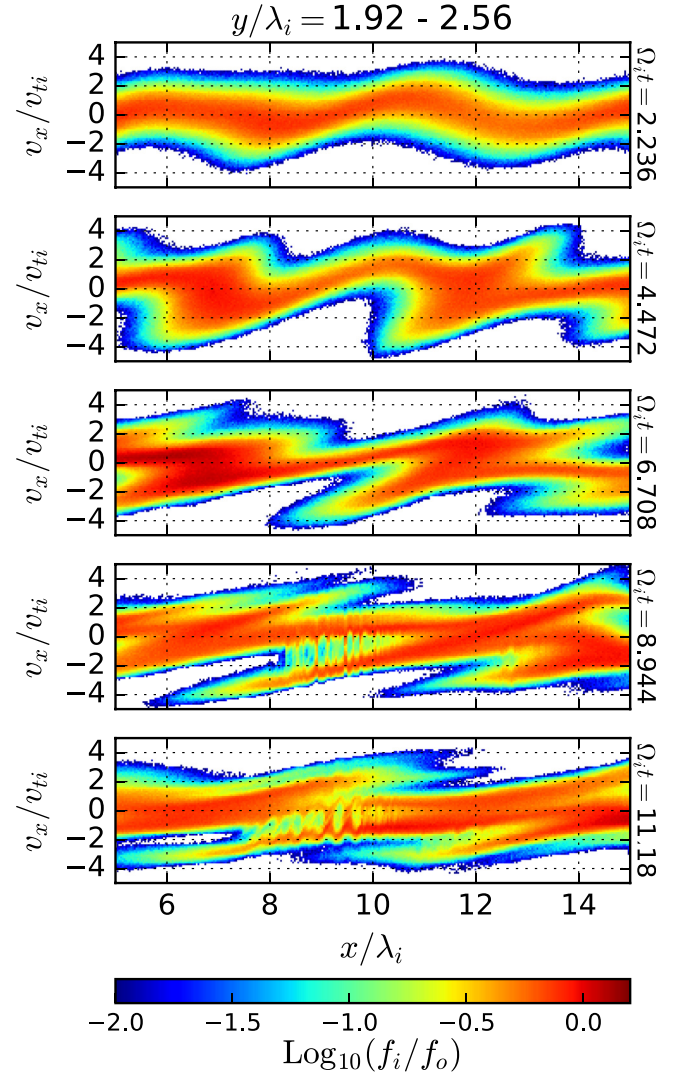
is defined as the velocity at the peak of the beam component. The beam density and the drift velocity monotonically increase with time. As beam density and velocity vary with time between $x/\lambda_i = 8.5$ and 9.5, the ion density fluctuations associated with the hole structures grow in between the beam and core components.

Figure 7 shows the $k_x - \omega$ diagram of δE_x along the field direction at $y/\lambda_i = 2.24$ between (a) $\Omega_i t = 0$ and 7.326 and between (b) $\Omega_i t = 7.326$ and 14.326. Here, the data line cuts through the center of the integration area transverse to the field direction ($y/\lambda_i = 1.92 - 2.56$) in Fig. 5. The ion acoustic speed C_s in the rest frame, indicated by dashed lines, can be expressed as

$$C_s = \left(\frac{k_B(T_e + 3T_i)}{m_i} \right)^{1/2}, \qquad (1)$$

where k_B is the Boltzmann constant. Note that the ion acoustic speed is calculated from the initial temperatures of the electrons and ions. The fluctuation amplitude of δE_x clearly
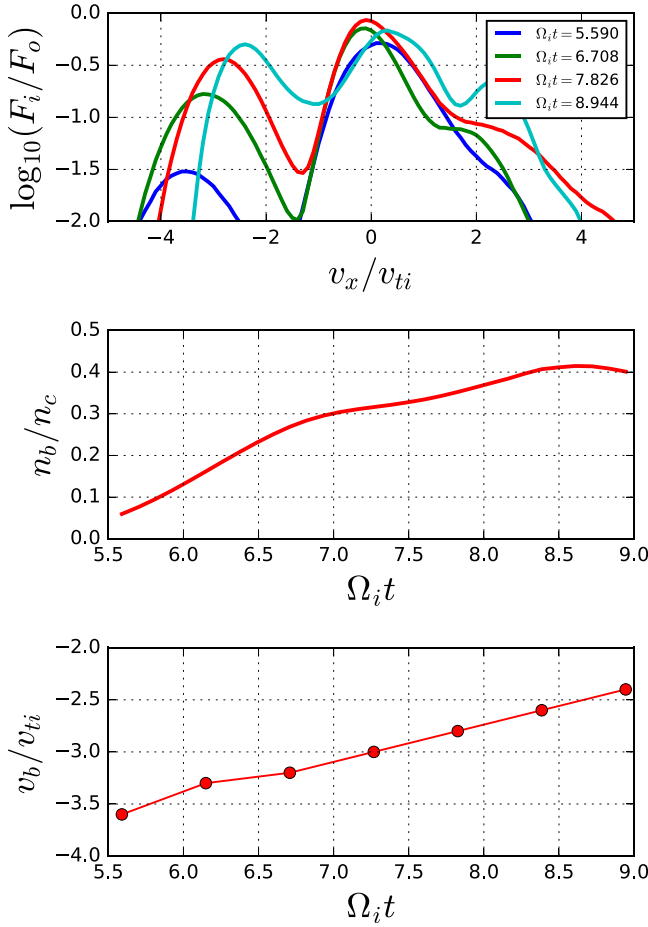
FIG. 6. (Top panel) Reduced ion velocity distributions that integrate the phase-space density shown in Fig. 5 over a range between $x/\lambda_i = 8.5$ and 9.5 at $\Omega_i t = 5.590$, 6.708, 7.826, and 8.944. (Middle panel) Density ratio for the beam and core components as a function of time. (Bottom panel) Time history of the drift speed of the beam component, where the beam drift speed is defined as the velocity at the peak of the beam component.

FIG. 7. Wavenumber-frequency diagram of δE_x along the x line at $y/\lambda_i = 2.24$ between (a) $\Omega_i t = 0$ and 7.326 and (b) $\Omega_i t = 7.326$ and 14.326. The field line is along the centerline of plotted area of Fig. 5. Dashed lines are ion acoustic speed C_s at $t = 0$. The fluctuation amplitude is normalized by the maximum value in the figure.

seen at $k_x\lambda_i < 2$ corresponds to the obliquely propagating whistler waves. At wavenumbers $k_x\lambda_i > 10$, the electric fluctuations $\delta E_x(k_x, \omega)$ grow at $\Omega_i t > 7.3$, whereas there is no quasi-parallel fluctuation at $\Omega_i t < 7.3$. The phase speed of all enhanced fluctuations at the short scales is slower than C_s. The fluctuations are broadly distributed at wavenumbers $k_x\lambda_i > 10$ and frequencies $\omega_r/\Omega_i < C_s k_x/\Omega_i$. In the following discussion, we explain that these enhanced fluctuations with phase speeds less than C_s are ion acoustic waves (IAWs) associated with the ion/ion acoustic instability.

III. DISCUSSION

Small-scale density fluctuations (Figs. 2–4) accompanied by electric fluctuations along the field direction (Fig. 7) grow in the regions where two ion components interact with each other (see Fig. 5). The bottom panel of Fig. 4 shows that the small-scale density fluctuations associated with the hole structures seen in Fig. 5 start to grow at $\Omega_i t > 8$. The temperature of the beam and core components is estimated to be $0.25T_{i,o}$ (Fig. 6). The density ratio of the two components and the drift speed of the beam component are found to be $n_b/n_c = 0.37$ and $v_b/v_{ti} = -2.7$ at $\Omega_i t = 8$. We
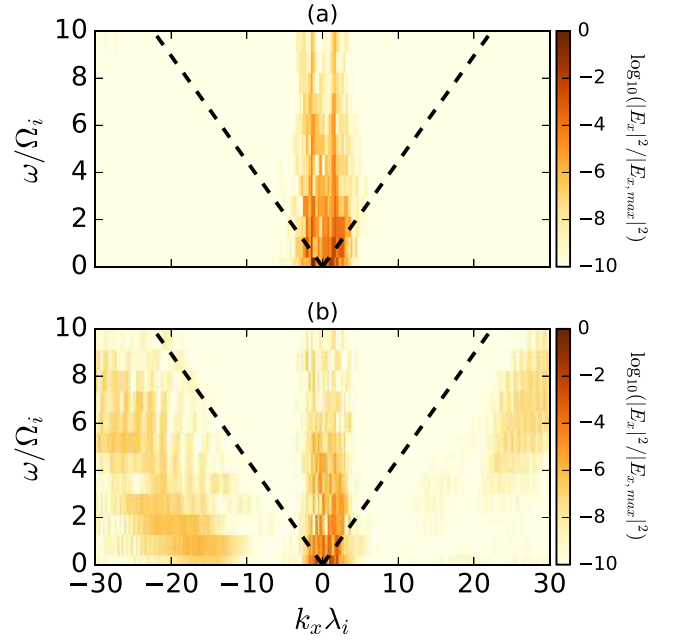
confirmed that the electron temperature in the region where the two distributions interact with each other is almost the same as its initial value, and therefore the electron temperature is larger than the ion temperature at $x/\lambda_i = 9$. With these parameter values, the local ion sound speed C_s normalized by the initial ion thermal speed is deduced to be 1.32. Substituting these parameter values into the equation for the ion/ion acoustic instability yields an empirical expression for the phase speed of the fastest-growing mode[25]

$$\frac{\omega_r}{k_x} \sim C_s \frac{n_c - n_b}{n_e}, \qquad (2)$$

where n_e is the background electron density and ω_r the real part of the angular frequency. Here, by assuming charge neutralization in the region, the electron density n_e is $n_c + n_b = n_e$. Hence, the phase speed of the growing mode is about $\omega_r/k_x = 0.6v_{ti}$. The wave frequency normalized by the ion cyclotron frequency can be rewritten as

$$\frac{\omega_r}{\Omega_i} = \frac{\omega_r}{k_x v_{ti}} \frac{v_{ti}}{v_A} k_x\lambda_i, \qquad (3)$$

so the normalized frequency is about $0.13k_x\lambda_i$, where $v_A/v_{ti} = 4.47$ (Sec. II A). The wavenumber of the growing mode is estimated as $k_x\lambda_i \sim 20$, which corresponds to a wavelength of about $\sim0.3\lambda_i$ [Fig. 3(B)] and therefore the frequency of the growing mode is $\omega/\Omega_i \sim 2.7$. This mode is included in the growing mode at $k_x\lambda_i \sim -20$ (Fig. 7). The implication is that the growing mode is an IAW driven by the ion/ion acoustic instability. Our simulation result shows that IAWs intermittently grow and decay in several regions within the turbulence (Fig. 4), indicating that this finite-amplitude whistler-mode turbulence may be the source of

intermittent growth of IAWs. IAWs may act to diffuse dynamically ion motion that may lead to dissipative effects in plasma turbulence. Such nonlinear developments of the phase-space density need careful study to understand dissipation within plasma turbulence at kinetic scales.

Our simulation demonstrates that whistler-mode turbulence decays, and thereby, the instability weakens over time ($\Omega_i t > 16$). However, if there is an energy source for whistler-mode turbulence at ion kinetic scales (for instance, turbulent cascade from MHD scales and/or wave growth by kinetic instabilities at ion kinetic scales), the patchy and intermittent generation of IAWs is to be expected to continue while the whistler-mode turbulence at ion kinetic scales evolves nonlinearly.

With the artificial mass ratio ($m_i/m_e = 100$) as described in Sec. II A, the IAWs generated by the ion/ion acoustic instability in our simulation have spatial scales larger than the electron inertial length. The artificial influence of the electron dynamics (e.g., the electron Landau process with a scale of order of the electron inertial length) on the IAWs is negligible in our simulation, and therefore, the artificial coupling between ions and electrons has a negligible contribution to the ion/ion acoustic instability. Hence, we expect that the growth of IAWs within whistler-mode turbulence observed in our kinetic simulation is strongly relevant to dynamics on solar-wind turbulence.

IAWs are considered to be enhanced in quasi-perpendicular collisionless shocks. Fredricks et al.[26] found that IAWs are strongly correlated with gradients in the magnetic field strength within the earth's bow shock. They expected a cross-field current of the gradients as a source of IAWs. One of the prime instabilities in the steep spatial gradient is the ion acoustic instability which drives waves propagating parallel to the electron drift in the cross-field current.[27] The observational results of Gurnett et al.[28] follow a linear theory suggesting that IAWs can grow in the plasma environment with a relatively large electron-to-proton temperature ratio T_e/T_p,[5,29] which supports the idea of an ion acoustic instability as a source of IAWs. Recent observations also indicate IAWs near the shock ramp region of a quasi-perpendicular interplanetary shock.[30] However, Thomsen et al.[31] noted that the thicknesses of the quasi-perpendicular bow shocks were generally not thin enough to trigger a cross-field ion acoustic instability, the thickness of which is about an ion inertial length.[32] This implies that the cross-field current is not the only process that generates IAWs around the shock front.

We believe that finite-amplitude whistler-mode turbulence may be a plausible source of the IAWs. Large-amplitude whistler waves are found in both Earth's bow shock[33] and interplanetary shocks.[34] Wilson et al.[34] also showed that the whistler waves in supercritical interplanetary shocks appear in a broad range of wavenumbers ($0.02 \leq k\rho_e \leq 5.0$) at the shock ramp. Here, ρ_e is the electron Larmor radius. Hybrid and particle-in-cell simulations[35] support the feature of finite-amplitude whistler waves growing in the foot region of supercritical perpendicular shocks. Whistler waves interacting with each other may develop in whistler-mode turbulence having broadband spectra as seen in observations.[34] From our simulation result, we propose that IAWs are enhanced intermittently in the finite-amplitude whistler-mode turbulence in the quasi-perpendicular collisionless shocks.

Whistler waves propagating in the oblique directions are enhanced by shock-reflected ions in the foot region through the modified two-stream instability.[36] However, it is not evident whether the instability can generate large-amplitude whistler waves as observed by the Wind spacecraft.[34] Self-consistent numerical simulations of quasi-perpendicular collisionless shocks obtained by resolving ion and electron kinetic scales are required to demonstrate IAW generation in shocks. Umeda et al.[37] have found IAWs in a quasi-perpendicular collisionless shock from a two-dimensional, fully kinetic, particle-in-cell simulation. However, as described in the paper, the underlying mechanism of generation remains unclear. The background magnetic field lines within the plane of the two-dimensional simulation box, so the cross-field ion acoustic instability,[27,29] which generates IAWs propagating along the cross-field current of the magnetic gradient, might be excluded from the generating mechanisms for IAWs in the simulation. The simulation suggests other sources for the IAWs in the collisionless shocks.

Whistler-mode turbulence leads to ion-density fluctuations at relatively large wavenumbers in the quasi-parallel directions with respect to the background magnetic field (Fig. 2). One may expect that the ion-density fluctuations are caused by interactions (for instance, $k_1 \rightarrow k_2 + k_3$) between initially applied whistler waves, similar to the decay instability of finite-amplitude Alfvén waves [e.g., Refs. 38 and 39]. However, the time scale of the growth of IAWs is much shorter than that of the time scale of the initially applied whistlers ($\sim 2\pi/\Omega_i$), so the wave interactions associated with whistler modes cannot be responsible for IAWs.

IV. SUMMARY

We performed a particle-in-cell simulation to examine the nonlinear dynamics of whistler-mode turbulence at ion kinetic scales. Our simulation shows that ion acoustic waves can be driven in whistler-mode turbulence through its nonlinear development of the phase-space density of ions along the direction of the background magnetic field. The ion acoustic waves grow intermittently in several regions, and the growth and damping of the wave packets occur over spatial scales greater than λ_i and over a time scale of Ω_i^{-1}. The wave generation is a result of a nonlinear response to whistler-mode turbulence at ion kinetic scales, and thus, the intermittent growth and damping of the ion acoustic waves would continue while the whistlers actively develop at these scales. We propose that the nonlinear development of the phase-space density that drives kinetic instabilities must be analyzed with greater care if the dissipation of plasma turbulence is to be understood. We believe that this nonlinear response is applicable in explaining the underlying IAW generation observed in the solar wind and the quasi-perpendicular collisionless shocks where whistler-mode turbulence develops nonlinearly.

[1] R. Leamon, C. Smith, N. Ness, W. Matthaeus, and H. Wong, "Observational constraints on the dynamics of the interplanetary magnetic field dissipation range," J. Geophys. Res. **103**, 4775, doi:10.1029/97JA03394 (1998).

[2] S. D. Bale, P. J. Kellogg, F. S. Mozer, T. S. Horbury, and H. Reme, "Measurement of the electric fluctuation spectrum of magnetohydrodynamic turbulence," Phys. Rev. Lett. **94**, 215002 (2005).

[3] F. Sahraoui, M. Goldstein, P. Robert, and Y. Khotyaintsev, "Evidence of a cascade and dissipation of solar-wind turbulence at the electron gyroscale," Phys. Rev. Lett. **102**, 231102 (2009).

[4] J. J. Podesta, J. E. Borovsky, and S. P. Gary, "A kinetic Alfvén wave cascade subject to collisionless damping cannot reach electron scales in the solar wind at 1 AU," Astrophys. J. **712**, 685 (2010).

[5] S. P. Gary, *Theory of Space Plasma Microinstabilities* (Cambridge University Press, 1993).

[6] F. V. Coroniti, C. F. Kennel, F. L. Scarf, and E. J. Smith, "Whistler mode turbulence in the disturbed solar wind," J. Geophys. Res. **87**, 6029, doi:10.1029/JA087iA08p06029 (1982).

[7] S. P. Gary and C. W. Smith, "Short-wavelength turbulence in the solar wind: Linear theory of whistler and kinetic Alfvén fluctuations," Geophys. Res. Lett. **114**, A12105, doi:10.1029/2009JA014525 (2009).

[8] Y. Narita, R. Nakamura, W. Baumjohann, K.-H. Glassmeier, U. Motschmann, B. Giles, W. Magnes, D. Fischer, R. B. Torbert, C. T. Russell, R. J. Strangeway, J. L. Burch, Y. Nariyuki, S. Saito, and S. P. Gary, "On electron-scale whistler turbulence in the solar wind," Astrophys. J., Lett. **827**, L8 (2016).

[9] S. Galtier and A. Bhattacharjee, "Anisotropic weak whistler wave turbulence in electron magnetohydrodynamics," Phys. Plasmas **10**, 3065 (2003).

[10] S. Dastgeer and G. P. Zank, "Anisotropic turbulence in two dimensional electron magnetohydrodynamics," Astrophys. J. **599**, 715 (2003).

[11] J. Cho and A. Lazarian, "The anisotropy of electron magnetohydrodynamic turbulence," Astrophys. J., Lett. **615**, L41 (2004).

[12] S. P. Gary, S. Saito, and H. Li, "Cascade of whistler turbulence: Particle-in-cell simulations," Geophys. Res. Lett. **35**, L02104, doi:10.1029/2007GL032327 (2008).

[13] S. Saito, S. Gary, H. Li, and Y. Narita, "Whistler turbulence: Particle-in-cell simulations," Phys. Plasmas **15**, 102305 (2008).

[14] S. P. Gary, S. Saito, and Y. Narita, "Whistler turbulence wavevector anisotropies: Particle-in-cell simulations," Astrophys. J. **716**, 1332 (2010).

[15] Y. Narita and S. P. Gary, "Inertial-range spectrum of whistler turbulence," Ann. Geophys. **28**, 597 (2010).

[16] S. Saito, S. P. Gary, and Y. Narita, "Wavenumber spectrum of whistler turbulence: Particle-in-cell simulation," Phys. Plasmas **17**, 122316 (2010).

[17] O. Chang, S. P. Gary, and J. Wang, "Whistler turbulence at variable electron beta: Three-dimensional particle-in-cell simulations," J. Geophys. Res. **118**, 2824, doi:10.1002/jgra.50365 (2013).

[18] S. Saito and Y. Nariyuki, "Perpendicular ion acceleration in whistler turbulence," Phys. Plasmas **21**, 042303 (2014).

[19] S. P. Gary, R. S. Hughes, and J. Wang, "Whistler turbulence heating of electrons and ions: Three-dimensional particle-in-cell simulations," Astrophys. J. **816**, 102 (2016).

[20] C. F. F. Karney and A. Bers, "Stochastic ion heating by a perpendicularly propagating electrostatic wave," Phys. Rev. Lett. **39**, 550 (1977).

[21] C. F. F. Karney, "Stochastic ion heating by a lower hybrid wave," Phys. Fluids **21**, 1584 (1978).

[22] T. Umeda, Y. Omura, T. Tominaga, and H. Matsumoto, "A new charge conservation method in electromagnetic particle-in-cell simulations," Comput. Phys. Commun. **156**, 73 (2003).

[23] O. Buneman, in *Simulation Techniques and Software*, edited by H. Matsumoto and Y. Omura (Terra Scientific, 1993).

[24] T. H. Stix, *Waves in Plasmas* (AIP Press, 1992).

[25] S. P. Gary and N. Omidi, "The ion/ion acoustic instability," J. Plasma Phys. **37**, 45 (1987).

[26] R. W. Fredricks, C. F. Kennel, F. L. Scarf, G. M. Crook, and I. M. Green, "Detection of electric-field turbulence in the earth's bow shock," Phys. Rev. Lett. **21**, 1761 (1968).

[27] S. P. Gary, "Longitudinal waves in a perpendicular collisionless plasma shock: II. Vlasov ions," J. Plasma Phys. **4**, 753 (1970).

[28] D. A. Gurnett, E. Marsch, W. Pilipp, R. Schwenn, and H. Rosenbauer, "Ion acoustic waves and related plasma observations in the solar wind," J. Geophys. Res. **84**, 2029, doi:10.1029/JA084iA05p02029 (1979).

[29] D. S. Lemons and S. P. Gary, "Current-driven instabilities in a laminar perpendicular shock," J. Geophys. Res. **83**, 1625, doi:10.1029/JA083iA04p01625 (1978).

[30] L. B. Wilson III, C. Cattell, P. J. Kellogg, K. Goetz, K. Kersten, L. Hanson, R. MacGregor, and J. C. Kasper, "Waves in interplanetary shocks: A wind/waves study," Phys. Rev. Lett. **99**, 041101 (2007).

[31] M. F. Thomsen, J. T. Gosling, and S. J. Bame, "Ion and electron heating at collisionless shocks near the critical Mach number," J. Geophys. Res. **90**, 137, doi:10.1029/JA090iA01p00137 (1985).

[32] C. T. Russell, M. M. Hoppe, W. A. Livesey, J. T. Gosling, and S. J. Bame, "ISEE-1 and 2 observations of laminar bow shocks: Velocity and thickness," Geophys. Res. Lett. **9**, 1171, doi:10.1029/GL009i010p01171 (1982).

[33] R. E. Holzer, T. G. Northrop, J. V. Olson, and C. T. Russell, "Study of waves in the earth's bow shock," J. Geophys. Res. **77**, 2264, doi:10.1029/JA077i013p02264 (1972).

[34] L. B. Wilson III, A. Koval, A. Szabo, A. Breneman, C. A. Cattell, K. Goetz, P. J. Kellogg, K. Kersten, J. C. Kasper, B. A. Maruca, and M. Pulupa, "Observations of electromagnetic whistler precursors at supercritical interplanetary shocks," Geophys. Res. Lett. **39**, L08109, doi:10.1029/2012GL051581 (2012).

[35] P. Hellinger, P. Trávníček, B. Lembège, and P. Savoini, "Emission of nonlinear whistler waves at the front of perpendicular supercritical shocks: Hybrid versus full particle simulation," Geophys. Res. Lett. **34**, L14109, doi:10.1029/2007GL030239 (2007).

[36] S. Matsukiyo and M. Scholer, "On microinstabilities in the foot of high Mach number perpendicular shocks," J. Geophys. Res. **111**, A06104, doi:10.1029/2005JA011409 (2006).

[37] T. Umeda, M. Yamao, and R. Yamazaki, "Cross-scale coupling at a perpendicular collisionless shock," Planet. Space Sci. **59**, 449 (2011).

[38] T. Terasawa, M. Hoshino, J. I. Sakai, and T. Hada, "Decay instability of finite amplitude circularly polarized Alfven waves: A numerical simulation of stimulated Brillouin scattering," J. Geophys. Res. **91**, 4171, doi:10.1029/JA091iA04p04171 (1986).

[39] H. Umeki and T. Terasawa, "Decay instability of incoherent Alfvén waves in the solar wind," J. Geophys. Res. **97**, 3113, doi:10.1029/91JA02967 (1992).